J. Fluid Mech. (1973), *vol.* 58, *part* 3, *pp.* 435–460
Printed in Great Britain

Wind-induced growth of mechanically generated water waves†

By W. STANLEY WILSON,‡ MICHAEL L. BANNER, RONALD J. FLOWER, JEFFREY A. MICHAEL AND DONALD G. WILSON

Chesapeake Bay Institute, The Johns Hopkins University

(Received 7 July 1972)

An experimental study was conducted to measure the growth rates of mechanically generated surface water waves when subjected to a fully developed turbulent channel airflow. The study was designed to test the accuracy of the growth rates predicted by Miles's (1962*b*) theory. For a series of wave frequencies (from 2·04 to 6·04 Hz at 0·50 Hz increments) and centre-line wind velocities (0·20, 1·12 and 1·84 m/s) wave amplitudes were measured at three stations (2·21, 3·43 and 4·65 m) downwind from a wave generator. In addition, for centre-line velocities of 1·12 and 1·84 m/s, U_1 (the velocity at the outer edge of the viscous sublayer) and U_* (the shear velocity) were obtained from measured mean velocity and Reynolds stress profiles. The wave amplitude measurements at the wind velocity of 0·20 m/s provided attenuation rate estimates which agreed reasonably well with theoretical attenuation rates based on viscous effects both on the walls and in the bulk of the water. The amplitude measurements at the wind velocities of 1·12 and 1·84 m/s provided growth rate estimates which were compared with theoretical growth rates (computed using the wave frequency, U_1 and U_*) predicted by Miles's (1962*b*) theory. At 1·12 m/s Miles's growth rates were two to five times larger than those measured; at 1·84 m/s Miles's growth rates were about two times larger.

1. Introduction

In a survey article Ursell (1956) presented a summary of the state of knowledge concerning the mechanism of wave generation which, in brief, can be described as highly inadequate. Since that time a number of wave generation theories have appeared. Phillips (1957) proposed a theory whereby the pressure fluctuations associated with the turbulence of a wind can generate waves on a previously flat water surface. This mechanism is characterized by producing linear growth for the waves.

Miles (1957, 1959*a*, 1962*b*) proposed two related theories, both of which require a previously wavy water surface to perturb the airflow. These are characterized by producing exponential growth for the waves. The first theory, Miles

† Contribution number 186 of the Chesapeake Bay Institute.

‡ Present address: Office of Naval Research, Code 481, Arlington, Virginia 22217.

(1957, 1959*a*), is concerned with relatively long waves ($c \gtrsim 10U_*$, where c is the phase velocity of the wave and U_* is the shear velocity of the airflow). For this case, the critical height, the height at which c equals the wind velocity, lies in the logarithmic region of the airflow. Several laboratory experiments have been conducted, but, at best, they show only qualitative agreement with this theory. Moreover, the applicability of this theory to the growth of waves in the ocean is questionable because field measurements have yielded growth rates an order of magnitude larger than those theoretically predicted. See Miles (1967) and Dobson (1971) for further discussion concerning these laboratory and field measurements.

The second theory, Miles (1962*b*), is concerned with relatively short waves ($c \lesssim 10U_*$). For this case the critical height lies in the viscous sublayer of the airflow. This particular theory was first considered in an unpublished work in 1952 by M. S. Longuet-Higgins. An independent study by Benjamin (1959) amplified the results, and Miles (1962*b*) developed them further (see Phillips 1966, p. 132). The study described herein is an experimental test of this theory, and it reviews a number of related experimental studies.

2. The theory

Miles's theory† considers the parallel shear flow of a light fluid (air) passing over the two-dimensional wave motion of a slightly viscous liquid (water). Equations for the wave motion, subjected to prescribed stresses at the surface, are obtained. Then the surface stresses produced by the parallel shear flow are calculated following the method of Benjamin (1959). Finally, the calculated stresses are matched across the surface and an eigenvalue equation for the complex wave speed is obtained. The solution to this equation provides the growth rate for the wave motion, expressed as a function of the frequency of the wave motion and the shear velocity and velocity at the outer edge of the viscous sublayer for the shear flow.

Miles's theory is based on the assumption that the turbulent characteristics of the airflow are functions only of height above the mean water level; this implies that the turbulence is not modified by the presence of waves on the water surface (Davis 1970). The only role that turbulence plays is to affect the shape of the mean velocity profile.

In the application of this theory to calculating wind-induced wave growth rates, the mean velocity profile in the viscous sublayer of the airflow is assumed to be linear in z and extends from the mean water level up to $z = \eta_1$, where $U(\eta_1) = U_1$, the velocity at the outer edge of the viscous sublayer. The mean velocity profile in the logarithmic region of the airflow is assumed to be

$$U(z) = U_1 + \frac{U_*}{\kappa}\left[\ln\left(\frac{4\kappa U_* z}{\nu_a}\right) - 1 + O(\eta_1/z)\right]. \tag{1}$$

Here U_* is the shear velocity (defined as the square root of the ratio of surface stress to density), κ is von Kármán's constant and ν_a is the kinematic viscosity. Based on results for turbulent flows over smooth solid surfaces (no accurate data

† Whenever the words 'Miles's theory' are used, they refer to Miles's (1962*b*) theory.

are available over water surfaces), the portion of the profile containing the viscous sublayer is below $z_* \equiv U_* z/\nu_a \simeq 5$ and the portion where (1) is applicable is above $z_* \simeq 30$. The transition region lies between these limits (see Hussain & Reynolds 1970; Monin & Yaglom 1971).

The wave motion is assumed to be of small amplitude and is represented by

$$\eta(x,t) = \eta_0 e^{ik(x-ct)},$$

where c = wave phase speed, k = wavenumber, x = direction of wave propagation and η_0 = initial wave amplitude. Furthermore, it is assumed that the direction of wave propagation is the same as the direction of the airflow and that there is negligible mean or shear flow in the water. In order to ensure that the critical eight η_c [where $U(\eta_c) = c$] lies in the viscous sublayer of the airflow, Miles's theory requires the wind velocity to be sufficiently fast so that

$$Z \equiv \left(\frac{k\nu_a}{U_*}\right)^{\frac{1}{3}} \frac{c}{U_*} < 2{\cdot}3. \tag{2}$$

In order to ensure that the Kelvin–Helmholtz mechanism (Miles 1959*b*) is not applicable, the wind velocity should be kept below 6·5 m/s.

3. Testing the theory

Under the restrictions outlined above, Miles's theory predicts the wind-induced wave growth rate for a single-frequency, unidirectional, small amplitude water wave when exposed to a sheared airflow blowing in the direction of wave propagation. For a particular wave frequency f and centre-line or reference velocity U_r for the airflow, a theoretical wind-induced wave growth rate can be calculated given the shear velocity U_* and the velocity U_1 at the outer edge of the viscous sublayer for the airflow. A corresponding experimental wind-induced wave growth rate can be calculated given the associated observed wave growth rate ζ and wave attenuation rate ζ_w. An experimental test of Miles's theory then has two natural parts: (i) a section on airflow measurements in which U_* and U_1 are measured for each U_r, and (ii) a section on water wave measurements in which ζ and ζ_w are measured for each f and U_r combination. Results from the first part then provide the information required to calculate the theoretical wind-induced growth rates and results from the second provide the experimental growth rates for comparison.

Airflow measurements

For this study a wind tunnel was coupled to a wave tank. A submerged oscillating cylinder generated waves mechanically in the tank, and a fully developed turbulent channel airflow was generated by the wind tunnel and directed over the waves. The fully developed turbulent channel type of airflow was chosen for a number of reasons. [For a more complete discussion see Laufer (1951), Comte-Bellot (1965) and Hussain & Reynolds (1970).] The basic characteristics of this airflow are independent of the downwind or axial co-ordinate and, away from the side walls, are independent of the cross-wind or transverse co-ordinate. This produces an approximately uniform wind stress on the wave field.

The shear velocity U_* for a particular centre-line wind velocity U_r can be obtained by using two properties of fully developed turbulent channel airflows: (i) the total stress profile is linear with height and (ii) the axial pressure gradient is constant (see Laufer 1951). Away from the walls and roof (where viscous stresses are important) and away from the water surface (where viscous and wave-induced stresses are important), the Reynolds stress will be the dominant contributor to the total stress and the Reynolds stress profile will be linear in height. An extrapolation of the Reynolds stress profile to the water surface yields U_*^2. If it is assumed that the airflow is two-dimensional in the mean and that the roof and water surface stresses are the same, the axial pressure gradient yields U_* according to

$$U_* = \left[\frac{d}{\rho_a}\frac{\partial p}{\partial x}\right]^{\frac{1}{2}}, \tag{3}$$

where d is the half-height of the air channel and ρ_a the air density. Note that these two methods for determining U_* are based on assumptions which are only approximately valid.

An additional property of fully developed turbulent channel airflow is that (1) is a good approximation to the logarithmic region (where $z_* \geqslant 30$) of the vertical mean velocity profile. When $U(z)$ is plotted with linear U against $\ln z$, the logarithmic region has a slope proportional to U_*. Consequently, any U_* (obtained from either of the two independent methods) can be used to fit a line with appropriate slope to $U(z)$, and U_1 can be computed as it is the only remaining unknown in the expression for $U(z)$. [Note that U_* and U_1 could both be determined using (1) – assuming the logarithmic region of $U(z)$ is *well defined.*]

Water wave measurements

Mechanically generated water waves closely approximate Miles's assumptions concerning a single-frequency, unidirectional, small amplitude wave motion. It might be possible to test his theory using *wind-generated* waves; however, as will be discussed in the next section, it is important to test the theory in such a manner as to most completely satisfy the theoretical assumptions. On the other hand, an evaluation of the theory with respect to its applicability to the growth of waves in the open ocean is a different question, and an experimental test directed toward this goal most certainly would use wind-generated waves.

The wind-induced growth rate is related to the observed growth rate (i.e. that growth rate computed using the observed wave amplitude distribution) by

$$\zeta = \zeta_a + \zeta_w, \tag{4}$$

where ζ = observed or total wave growth rate, ζ_a = wind-induced or net wave growth rate and ζ_w = wave attenuation rate, a negative term. When there is no wind blowing over the waves, $\zeta_a = 0$ and $\zeta = \zeta_w$.

The observed wave growth rate is related to the amplitude distribution of the wave field by

$$\overline{(\eta(x)^2)}^{\frac{1}{2}} = \overline{(\eta_0^2)}^{\frac{1}{2}} e^{\zeta x/c_g},$$

where c_g is the wave group speed, and to the complex phase velocity $c + ic_i$ of the wave field by $\zeta = kc_i$ (see Miles 1962*b*). $\overline{\eta(x)^2}$ represents an amplitude averaged

over both time and transverse direction, at a constant fetch. In practice, the observed wave growth rate was computed between successive positions in the downwind direction (x) using

$$\zeta = kc_i = \frac{c_g}{x_2 - x_1} \ln\left(\frac{(\overline{\eta(x_2)^2})^{\frac{1}{2}}}{(\overline{\eta(x_1)^2})^{\frac{1}{2}}}\right). \tag{5}$$

The theoretical wave attenuation rate ζ_w is obtained using

$$\zeta_w = -2\nu_w k^2 - \frac{2kc_g}{b}\left(\frac{\nu_w}{2f}\right)^{\frac{1}{2}}, \tag{6}$$

where b is the separation of the side walls and ν_w the viscosity of the water. The first term on the right-hand side accounts for the viscous dissipation due to the bulk of the fluid, and the second accounts for the viscous dissipation due to the presence of the side walls. [See Ursell (1952) and Benjamin & Ursell (1954) for viscous dissipation due to bulk and side wall effects. Hunt (1952) has extended the theory to include bottom effects, but they are negligible for this study.]

4. Previous experimental work

There have been four previous experimental studies attempting to test Miles's theory. Two of them (Hidy & Plate 1966; Sutherland 1968) used wind velocities sufficiently fast ($6 < U_r < 15$ m/s) to produce wind-generated water waves; no waves were mechanically generated. They recorded wave amplitudes at various stations in the downwind direction and computed spectra for the records. Experimental wave growth rates were then calculated for different spectral components. Theoretical wave growth rates were calculated using a U_* obtained from a measured mean velocity profile and an assumed value for U_1. In addition to the fact that their experimental wave growth rates were fetch dependent and that their theoretical growth rates were not rigorously determined, there are a number of other disadvantages to this type of experimental approach. It is unlikely that the small amplitude assumption is maintained with wind-generated waves. The possibility of the airflow separating at the crests is increased with finite amplitude waves. There is no control on the frequency and direction for wind-generated waves. These wind speeds are fast enough to provide an opportunity for the Kelvin–Helmholtz mechanism to occur. There are increased possibilities for wave–wave interactions with wind-generated waves. As was stated in the previous section, it is crucial to match the experiment with the theory and the best experimental test is the simplest and cleanest test, that using single-frequency, unidirectional, small amplitudewaves. Consequently, their results will not be compared with those from this study.

The third experimental study (Hires 1968) used mechanically generated waves which satisfied Miles's assumptions. Experimental growth rates were obtained for five wave frequencies (4·00, 4·25, 4·50, 4·80 and 5·20 Hz) and one wind velocity (1·20 m/s). A Reynolds stress profile was used to estimate U_*. Unfortunately, a mean velocity profile was not measured, and as a result no reliable estimate was available for U_1. In order to compare his experimental results with Miles's theory,

a floating parameter ($= U_1/U_*$) was introduced, and its value was adjusted until his theoretical growth rates gave a 'best fit' to his experimental growth rates. Although his study did not provide a clear test of Miles's theory, his results will be compared with the results of this study in a later section.

The fourth experimental study (Gottifredi & Jameson 1970) also used mechanically generated waves. Experimental growth rates were obtained for four wave frequencies (3·85, 4·61, 6·20 and 7·62 Hz) and approximately six wind velocities ($0{\cdot}8 < U_r < 4{\cdot}9$ m/s). Mean velocity profiles were measured for the different wind velocities, and straight lines were fitted to a log–linear plot of each profile to obtain both U_* and U_1. (Experiments were conducted using water, glycerol solutions and sodium lauryl sulphate solutions; however, only the results for the case of water will be considered here.)

Unfortunately, the design of this experiment (Gottifredi & Jameson 1970) and the quality of the measurements leave a great deal to be desired. The airflow used for the study was not fully developed, so that for each U_r different values of U_1 and U_* were obtained for different fetches. (The experimental wave growth rates were similarly fetch dependent.) Furthermore, a Pitot-static tube was used to obtain the mean velocity profiles and no corrections were made for velocity-gradient or turbulence-level effects (see, for example, Ower & Pankhurst 1966, pp. 45–48). In observing the mean velocity profiles, there is no *obvious* linear region on the log–linear plots to which a straight line (used to yield a U_* and U_1) can be reasonably fitted. There were other problems such as taking all wave amplitude measurements in the centre of the tank without demonstrating lateral uniformity. Although little reliance can be placed on their study, the results will be compared with the results of this study in a later section.

5. The wind–wave facility

The wind–wave facility, previously used by Hires (1968), consisted of a wind tunnel coupled with a wave tank (see figure 1). Three rows of coiled springs were attached to both the roof and floor just after the contraction in order to reduce the wall jets induced by the contraction and to vigorously initiate turbulent boundary layers at a point 72 channel heights upstream from the working section. This assured ample opportunity for the turbulent boundary layers to grow, merge together and produce a fully developed turbulent channel flow at the working section of the wave tank.

To produce a constant (steady) wind velocity in the working section of the channel of the wave tank, it was necessary to regulate the speed of the fan and the temperature of the air. The humidity of the air remained between 70 and 80 % relative humidity, so it was not necessary to control it. The fan speed was maintained to within ± 1 %. A thermistor mounted in the working section of the air channel sensed temperature, and by using a heater and air conditioner, the air temperature was kept within the desired limits, which will be discussed below.

The frequency of the wave generator was controlled to within $\pm 0{\cdot}3$% (see figure 2).

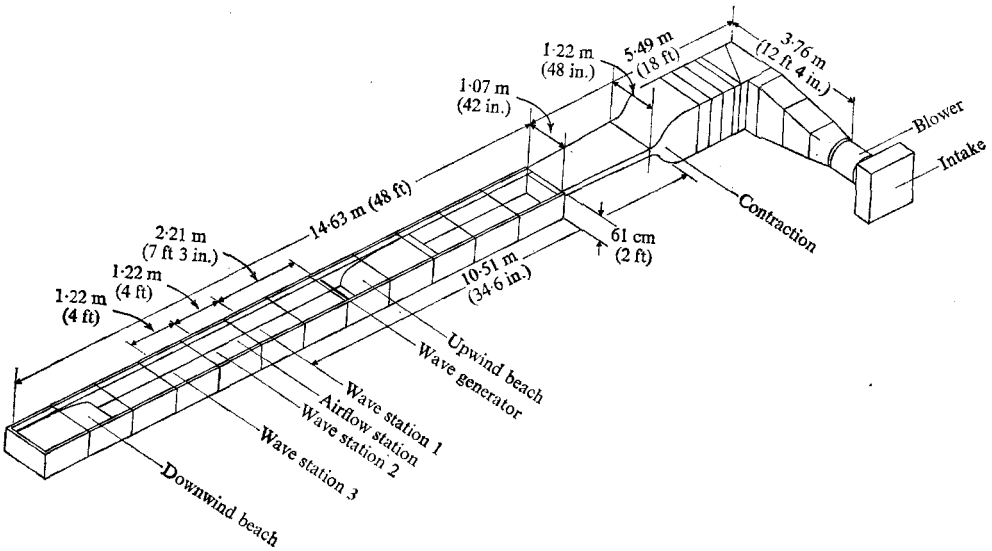

FIGURE 1. The wind–wave facility (after Hires 1968).

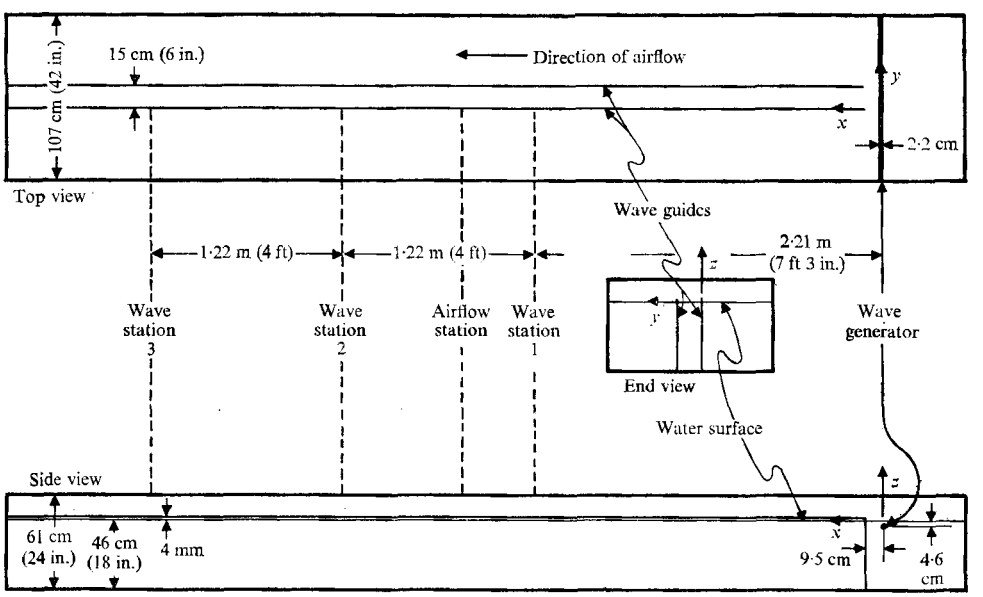

FIGURE 2. The working section of the wave tank in which the experimental measurements were taken.

A 15·24 cm wide wave-guide channel was installed in the tank. It extended from 4 mm above the water surface to the bottom of the tank and from just after the wave generator to the downwind beach. One reason for installing the wave-guide channel was to isolate a portion of the wave field over which wind conditions, particularly the surface stress, would be relatively uniform in the cross-tank direction. Another reason was related to the variation of time-averaged wave amplitudes in the cross-tank direction, i.e. the absence of lateral uniformity.

Much sampling in the cross-tank direction was required to obtain a repeatable amplitude distribution at a given fetch. By restricting measurements to the wave-guide channel – as opposed to the entire wave tank – significantly less sampling was necessary.

A standpipe drain was installed at the downwind end of the tank. By continually adding water to the tank (about 3 l/min) and by constantly blowing wind over the water surface (at least 0·2 m/s), surface contaminants were blown to the downwind end of the tank and skimmed off by the standpipe. The problem of surface contamination and its effect on wave attenuation will be discussed below.

6. Airflow measurements

Instrumentation

Hot-wire anemometers using two basic sensors were used to measure the airflow. One sensor was a mean-velocity single-wire probe (TSI 1274-T1.5) having a tungsten sensing element 0·0038 mm in diameter and 1·27 mm in length. The second was a Reynolds-stress X-wire probe (TSI NTX-T1.5) having two tungsten sensing elements separated by 1·27 mm, each element having the same diameter and length as the single-wire probe. Both sensors were driven at a 1·6 overheat ratio, using modified constant-temperature anemometers (TSI 1010) and linearizers (TSI 1005B). These gave a linear output of approximately 1 V/ms^{-1}.

For Reynolds stress measurements the two linearized outputs ($\alpha u \pm \beta w$) were fed into an adder–subtracter unit giving $2\alpha u$ and $2\beta w$. These were high-pass filtered, multiplied together, integrated and scaled to give $\overline{u'w'}$.

For hot-wire calibration a portable wind tunnel was used *in situ* to ensure similar calibration and measurement environments. It has a 10:1 area contraction, a 3·5 cm square working section, and turbulence level $[\overline{u'^2}]^{\frac{1}{2}}/U < 0{\cdot}003$.

The hot-wire anemometer systems were calibrated with this tunnel at five velocities (0·64, 1·07, 1·71, 2·48 and 3·50 m/s). A Pitot-static tube was used to set the fastest velocity (U). A cylinder (with diameter D) was inserted normal to the flow direction, and the frequency N of eddies shed from one side of the cylinder was counted. This gave a characteristic Reynolds number ($R \equiv UD/\nu_a = 68$) and Strouhal number ($S \equiv ND/U = 0{\cdot}133$). Given the relatively flat velocity profile in the working section of the calibration tunnel, a constant-diameter vortex-shedding cylinder and a low Reynolds number, a unique relationship exists between R and S (see Gaster 1971). Thus, to calibrate the tunnel at the lower four speeds for which the Pitot-static tube is relatively inaccurate, appropriate cylinder diameters and corresponding eddy-shedding frequencies were calculated. To set the tunnel at one of the lower speeds, a cylinder with appropriate diameter was inserted in the tunnel and the fan speed varied until the corresponding eddy-shedding frequency was achieved. Full details, including a sample calibration curve, are given by Wilson (1972).

The Reynolds stress X-wire probe gave two linearized output voltages, $E = \alpha u \pm \beta w$, where

$$\alpha \equiv \frac{\Delta E}{\Delta u}\bigg|_{\theta=\text{constant}}, \quad \beta \equiv \frac{1}{u}\frac{\Delta E}{\Delta \theta}\bigg|_{u=\text{constant}} = \frac{\Delta E}{\Delta w},$$

and for calibration the probe is oriented with the plane of the X-wire horizontal. The algebraic sign of the second term in the expression for E depends on the sign of θ (the angle between a particular wire and the flow direction), where, for measurement use, $\theta = \pm 45°$. Complications occur in calibrating X-wire probes because an α and β can be measured for each wire with the plane of the X-wire in one orientation (non-inverted) and for each wire again with the plane of the X-wire rotated through 180° about the flow direction (inverted orientation). To ensure a meaningful calibration, it is critical to match the corresponding α's and the corresponding β's as closely as possible.

For calibration each anemometer was linearized with the X-wire probe in the non-inverted orientation with $\theta = 45°$ for wire 1 and $\theta = -45°$ for wire 2. At a constant calibration velocity the probe was yawed until $\theta = 90°$ (wire 1 perpendicular to the flow) and the linearized voltage was noted for wire 1. The probe was then yawed until $\theta = 0°$ (wire 2 perpendicular to the flow) and the linearized voltage for wire 2 was adjusted to equal that value for wire 1 at $\theta = 90°$. This set the α's equal. Values of β were then measured for each wire at a particular speed by yawing the X-wire probe $\pm 5°$ about $\theta = 45°$. After a β had been determined for one or more speeds for each wire, the X-wire probe was flipped to its inverted orientation and the α and β values were noted for comparison. Values of α and β measured with the X-wire probe in the non-inverted orientation changed by less than 2% when the probe was flipped to its inverted orientation. Variation of β over the entire speed range for the Reynolds stress measurements ($0{\cdot}9 < U < 1{\cdot}8$ m/s) was less than 2%.

Procedure

All hot-wire measurements were taken at the transverse centre-line (i.e. $y = 7{\cdot}62$ cm) of the airflow station shown in figures 1 and 2 using the mean water level as the reference level (i.e. $z = 0$). Three or four 2 min integration averages were obtained at each height in order to estimate both the mean velocity and Reynolds stress.

After calibration with the X-wire in the horizontal plane, the probe was rotated through 90° to set the X-wire in the vertical plane. The pitch was adjusted to give a zero mean voltage difference between the two wires. After the set of Reynolds stress measurements had been obtained, the X-wire was inverted, the pitch was similarly adjusted and the set of measurements was duplicated.

The hot wires were calibrated at $21{\cdot}3 \pm 0{\cdot}1$ °C and the centre-line airflow temperature was kept within these same limits. When the single-wire probe was to be used for measuring a $U(z)$ profile, the temperature at the midpoint of the logarithmic region ($0{\cdot}6 < z < 3{\cdot}0$ cm) of the airflow was measured and the values of α and β corrected for that temperature and assumed constant over the logarithmic region. The maximum temperature difference over the entire logarithmic region was less than 0·3 °C, and the error in α and β introduced by the temperature variation was less than $\pm \frac{1}{4}$%. When the X-wire probe was to be used for measuring a Reynolds stress profile, the calibrated values of α and β were appropriate for the centre-line temperature and assumed constant over the region of Reynolds stress measurements. The maximum temperature difference over this region

($1 < z < 13$ cm) was less than 0·7 °C, and the error in α and β was less than $\pm \frac{1}{2}\%$. Consequently, the errors introduced by assuming no temperature variation with height were neglected.

Because Miles's theory assumes a neutrally stable airflow over the waves, it is desirable to minimize the difference between the temperature at the airflow centre-line (θ_r) and at the water surface (θ_s). Hires (1968) presents arguments to suggest that $\theta_r - \theta_s < \pm 2{\cdot}3$ °C is sufficient to achieve neutral stability. Although it was possible to control the centre-line airflow temperature, it was not possible to control the water temperature. It was only indirectly controlled by controlling the airflow temperature. For all wave measurements in this study,

$$2{\cdot}2 < \theta_r - \theta_s < 3{\cdot}2\,°\text{C} \quad \text{and} \quad 21{\cdot}2 < \theta_r < 22{\cdot}1\,°\text{C}.$$

For all airflow measurements in this study,

$$0{\cdot}7 < \theta_r - \theta_s < 1{\cdot}7\,°\text{C} \quad \text{and} \quad \theta_r = 21{\cdot}3 \pm 0{\cdot}1\,°\text{C}.$$

It was assumed that these temperature differences did not affect the neutral stability of the airflow.

Estimates of U_* for each U_r were obtained by using the X-wire probe to measure a vertical Reynolds stress profile, fitting a straight line to the data and extrapolating the line to the water surface to get U_*^2. The results were checked by using a micromanometer to measure the axial pressure gradient along the centre-line at the roof. Although the distance over which the gradient was estimated was rather large (5·9 m), the pressure differences used with equation (3) were rather small, and this was not a particularly accurate way of estimating U_*.

Results

A typical Reynolds stress profile, corresponding to $U_r = 1{\cdot}84$ m/s, is given in figure 3. In order to note how these measurements were affected by water waves, some measurements were taken when no waves were present on the water surface (denoted by 'NW' in the figures) and some when 3·54 Hz waves were present. [This particular frequency was chosen because, over the entire wave frequency range used in this study, these waves have the maximum amplitude.] As can be seen in figure 3 (and similarly in the profile for $U_r = 1{\cdot}12$ m/s given by Wilson 1972) the Reynolds stress profiles are not significantly affected by waves on the water surface.

The average of the inverted and non-inverted X-wire probe values was taken at each height (and denoted by a cross), and a line was fitted by eye to these average values. The slight systematic discrepancy between the values for the non-inverted and inverted positions is probably due to asymmetry of the two wires in the X-wire probe. As anticipated for fully developed turbulent channel flow, the Reynolds stress profiles appear to be linear in z and have an approximately zero value at the centre-line.

A mean velocity profile corresponding to $U_r = 1{\cdot}84$ m/s is given in figure 4. For $U_r = 1{\cdot}12$ m/s the mean velocity profile above 0·3 cm was not significantly affected by waves on the water surface. However, for $U_r = 1{\cdot}84$ m/s there was a slight effect. For $z = 0{\cdot}7$ cm, $U \approx 130$ cm/s when 3·54 Hz waves were present

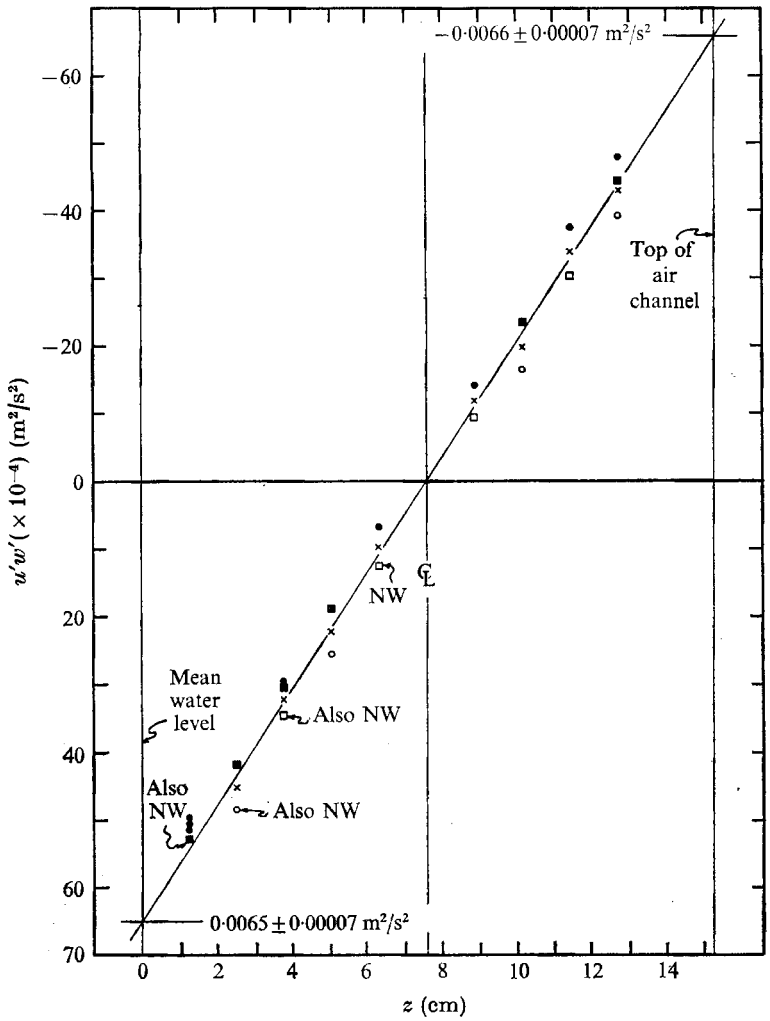

FIGURE 3. Reynolds stress $\overline{u'w'}$ for centre-line wind velocity of 1·84 m/s expressed as a function of height z above mean water level. Probe orientation: ●, inverted, 8 July 1971; ■, inverted, 9 July 1971; ○, non-inverted, 8 July 1971; □, non-inverted, 9 July 1971. ×, average of inverted and non-inverted values. All measurements made with 3·54 Hz waves on water surface unless marked 'NW' (no waves on surface).

and $U \approx 133$ cm/s with no waves present. For $z > 1{\cdot}5$ cm there was no change noted in U. Note that the waves only affect the lower portion of the logarithmic region. The maximum change to be expected in calculating U_1, from the case of maximum amplitude waves to the case for no waves, is an increase of 2 or 3 cm/s. As will be seen below, this change is smaller than the uncertainty in determining U_1. Consequently, this effect has been neglected.

Estimates of U_* obtained from both the Reynolds stress and the axial pressure gradient measurements – as well as a U_* representing the average of both – are given in table 1 for each U_r. An estimate of U_1 and of the ratio U_1/U_* corresponding to each U_* estimate is also given. The value of z for $z_* = 30$ (the lower limit of

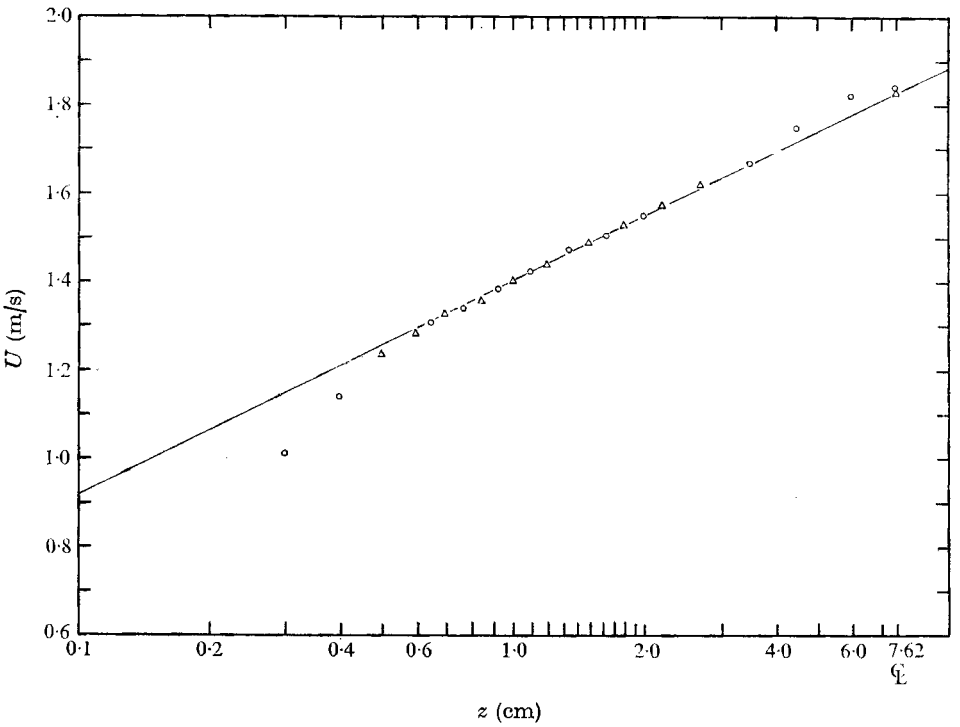

FIGURE 4. Axial component U of mean wind velocity for centre-line wind velocity of 1·84 m/s expressed as a function of height z above mean water level. △, 3 August 1971; ○, 5 August 1971. Slope of line corresponds to $U_* = 8{\cdot}4$ cm/s, $\kappa = 0{\cdot}4$. All measurements made with 3·54 Hz waves on water surface.

U_r (m/s)	U_* (cm/s)	U_1 (cm/s)	U_* method	U_1/U_*
1·12	5·2 ± 0·5 %	43·8	Reynolds stress	8·4
	5·3	42·4	Average of both	8·0
	5·4 ± 3·5 %	41·3	Pressure gradient	7·6
1·84	8·1 ± 0·5 %	70·1	Reynolds stress	8·7
	8·4	66·7	Average of both	7·9
	8·7 ± 1·5 %	63·1	Pressure gradient	7·3

TABLE 1

the logarithmic region of the profile) at which $U_r = 1{\cdot}12$ m/s is about 8·3 mm and that at which $U_r = 1{\cdot}84$ m/s is about 5·3 mm. The value of z for $z_* = 5$ (the upper limit of the linear region of the mean velocity profile) at which $U_r = 1{\cdot}12$ m/s is about 1·4 mm and that at which $U_r = 1{\cdot}84$ m/s is about 0·9 mm. For comparison, the variation of the root-mean-square wave amplitudes satisfied $0{\cdot}01 < \overline{\eta^2} < 0{\cdot}30$ mm over the entire wave frequency and wind velocity range used in this study.

7. Wave growth rates predicted theoretically

Miles's theory predicts a wind-induced or net wave growth of the form

$$\zeta_a = \frac{\rho_a}{\rho_w}\frac{U_*^2}{2\nu_a}\left[\frac{-F_i-(\nu_a k/U_*)^{\frac{2}{3}}(w_r-F_r)H_i}{(F_r-w_r)^2+F_i^2}\right], \tag{7}$$

where $\rho_a/\rho_w = 0{\cdot}00121$, the ratio of the densities of air and water, and

$$\nu_a = 0{\cdot}148\,\mathrm{cm^2/s},$$

the kinematic viscosity of air. This equation has been obtained by taking Miles's (1962*b*) equation (7.3*b*), substituting for terms using his equations (3.4) and (7.4), and setting $w_i = 0$ using his equations (3.10) and (8.1). Values for F_i, F_r and H_i (each a function of Z) were obtained from his figure 3, where Z is defined in our equation (2). [This definition of Z comes from his equations (3.4), (3.9) and (7.4).] Values for w_r appearing above in our equation (7) were calculated following the method outlined by Miles (1962*a*). This involves taking his equations (5.11) and (5.12) as an approximation to his equation (5.9). In order to check the above technique for computing ζ_a, sample calculations using Miles's (1962*b*) input data were performed, and the results duplicated those given in his figure 5.

Three wind-induced wave growth rate (ζ_a) curves were calculated for each U_r; they are associated with the three pairs of (U_*, U_1) values given above for each U_r and reflect the uncertainty introduced in the determination of ζ_a due to measurement error. These results are plotted in the final figure (figure 14).

The restrictions imposed by Miles's theory on the results of this study are

$Z < 2{\cdot}3$ from our equation (2),

$|U_1 - c| \gg c_i$ from Miles (1962*b*) equation (5.4*b*), and

$U_1 - c \geqslant U_*$ from Miles (1962*a*, p. 432).

A sufficient condition for these three restrictions to be satisfied is

$$f \begin{cases} > 4{\cdot}54\,\mathrm{Hz} & \text{for } U_r = 1{\cdot}12\,\mathrm{m/s}, \\ > 3{\cdot}04\,\mathrm{Hz} & \text{for } U_r = 1{\cdot}84\,\mathrm{m/s}. \end{cases}$$

8. Water wave measurements

Instrumentation

Measurements of water wave amplitudes were made with a set of three 'impedance-type' wave probes each using a 0·0375 mm diameter bare tungsten wire which hangs partially immersed in the water. This wave probe system is similar to that described by McGoldrick (1965) and used both by Hires (1968) and McGoldrick (1970).

The three output signals from the wave probes were amplified to scale their gains to be 1·23 V/mm, were high-pass filtered to provide a stable zero mean and were amplified again either 3 or 6 times. Static calibrations of the wave probes at 0·25 mm increments over a total range of 20 mm showed excellent linearity.

Dynamic calibrations were performed by vertically oscillating a wave probe in a sinusoidal manner in a tank of still water. A precision potentiometer, coupled to the probe, provided a reference signal for comparison with the output from the probe. Calibrations were performed at an oscillation frequency of 3·24 Hz and oscillation amplitudes (root-mean-square) of 0·14, 0·21 and 0·28 mm. The output from both the probe and potentiometer were simultaneously sampled and then digitally processed. Root-mean-square amplitudes, computed from probe and potentiometer output data records, differed by less than $2\frac{1}{2}\%$ for 0·14 mm and $1\frac{1}{2}\%$ for 0·21 and 0·28 mm amplitude oscillations. Unfortunately, mechanical vibrations in the system prevented making dynamic calibrations at smaller oscillation amplitudes.

The three wave probe output signals were simultaneously digitized at a 16 Hz sampling frequency and converted into a series of numbers with 9 binary bits, which provide a range-to-resolution ratio of 512 to 1. A least count (20 m V/count) corresponds to 0·0031 mm of water for 6 and 0·0062 mm for 3 times amplification. The digitized wave signals were then fed to a computer-compatible incremental magnetic tape recorder. Data processing, including spectral computations, was then performed by a computer.

Procedure

The lower bound to the range of wave frequencies ($2{\cdot}04 < f < 6{\cdot}04$ Hz) used in this study was chosen to avoid shallow-water effects ($h < \lambda$) and to ensure that the wind-induced wave growth rates would be negligible for the lowest frequency waves. The latter condition was a consistency check: the observed wave growth rate for the lowest frequency waves should be the same for all of the wind velocities used in the study. The upper bound was set by the waves themselves: higher frequency waves had such small amplitudes that they could not be accurately measured with the wave probe system.

Over the entire wave frequency and wind velocity range used in this study, the wave slopes satisfied $0{\cdot}005 < \eta k < 0{\cdot}03$, certainly satisfying the small amplitude requirement.

The wave probes were used at the three stations indicated in figures 1 and 2. At each station there were eleven positions, evenly spaced across the wave-guide channel, used for measuring wave amplitudes. An experimental run for wave attenuation rate measurements consisted of using a wave probe simultaneously at each of the three stations and obtaining a 250 s long record corresponding to each of the eleven positions. Each record was digitized, the variance calculated, 'system noise' subtracted if necessary and the root-mean-square amplitude computed. Results at this stage consisted of an eleven-point wave amplitude distribution for each of the three stations. An average amplitude was then computed for each station, and one observed growth rate calculated between the first pair of stations and another between the second pair using (5). The two resulting growth rates provided a consistency check to demonstrate possible fetch dependence.

An experimental run for wind-induced growth rate measurements also consisted of using a wave probe simultaneously at each of the three stations. The only difference was a considerably longer recording time necessary to ensure

f (Hz)	U_r (m/s)	'Spike' bandwidth (Hz)	Fraction of variance (%)
$2 \rightarrow 6$	0·20	0·04	99
$2 \rightarrow 4\frac{1}{2}$	1·12	0·04	99
$2 \rightarrow 3$	1·84	0·04	99
5	1·12	0·04	94
		0·12	99

TABLE 2

repeatability. A 750 s long time series corresponding to each of the eleven positions was recorded; then two more similar passes across the eleven positions were recorded.

The 'system noise' referred to above simply means the variance or root-mean-square amplitude of the time series from an experimental run conducted with the wind blowing but the mechanically generated waves not present. For the three centre-line wind velocities $U_r = 0{\cdot}20$, 1·12 and 1·84 m/s, it amounted to $(\overline{\eta^2})^{\frac{1}{2}} =$ 0·002, 0·008 and 0·010 mm respectively. It is interesting to note that when time series taken only of 'system noise' are Fourier transformed the spectra are relatively flat or white and do not have any significant peaks corresponding to spontaneous wind-generated waves.

It is also interesting to note that Fourier transforms taken of regular experimental runs were characterized by being flat at all frequencies away from the frequency of the mechanically generated waves. At this frequency a 'spike' appears in the spectra; the bandwidth of the 'spike' increases as the wave frequency increases, the wind velocity increases and to a very slight extent as the fetch increases. (For this study the wave frequencies were selected to coincide with the frequencies of individual Fourier coefficients.) The results in table 2 show the fraction of the total variance of a record accounted for by the indicated 'spike' bandwidth.

The results indicate that, with the exception of the small amount of 'system noise' which was removed, all of the energy of the records was centred on and associated with the frequency of the mechanically generated waves. As a result, neither band-pass filtering nor Fourier transforming was performed in the routine analysis of the data for this study.

Results

Typical results of the wave amplitude measurements, expressed in the form of amplitude distributions within the wave-guide channel, are presented in figures 5–9. Note in figures 6, 7 and 8 that the distributions, although smoothly changing for the most part, are quite irregular.

There is no apparent explanation for the strange amplitude distributions. Although the frequencies used in this study were chosen to avoid the resonance frequencies in the transverse or cross-wave-guide direction (3·22 Hz for the fundamental, 4·64 and 5·84 Hz for the lower two harmonics), a partial resonance of this type might have occurred. Another possibility might be contamination of

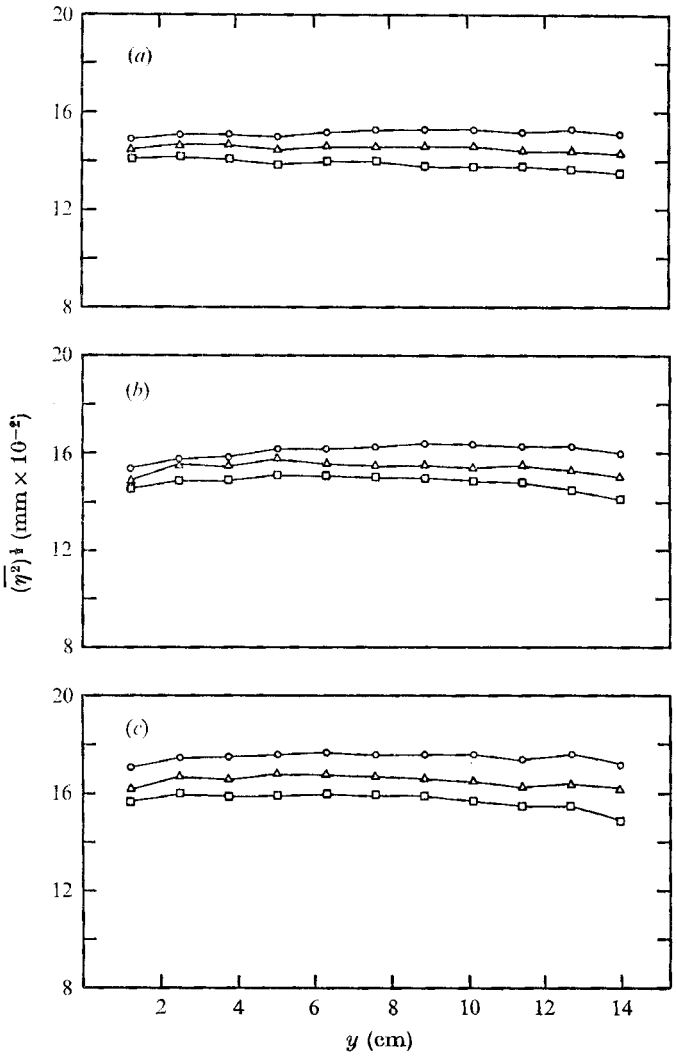

FIGURE 5. Root-mean-square amplitude $(\overline{\eta^2})^{\frac{1}{2}}$ for 2·04 Hz waves expressed as a function of centre-line wind velocity U_r, transverse position y in wave-guide channel and downwind distance x from wave generator. Wave guides are located at $y = 0$ and 15·24 cm. ○, $x = 2{\cdot}21$ m; △, $x = 3{\cdot}43$ m; □, $x = 4{\cdot}65$ m. (*a*) $U_r = 1{\cdot}84$ m/s, run 137*B*. (*b*) $U_r = 1{\cdot}12$ m/s, run 146. (*c*) $U_r = 0{\cdot}20$ m/s, run 149.

the primary wave train by waves of the same frequency which were generated where the submerged oscillating cylinder meets each lateral wall of the wave tank. Sometimes these waves were barely visible, with their crests radiating in a semicircular pattern on the surface near each end of the oscillating cylinder, and energy associated with them might have entered the wave-guide channel.

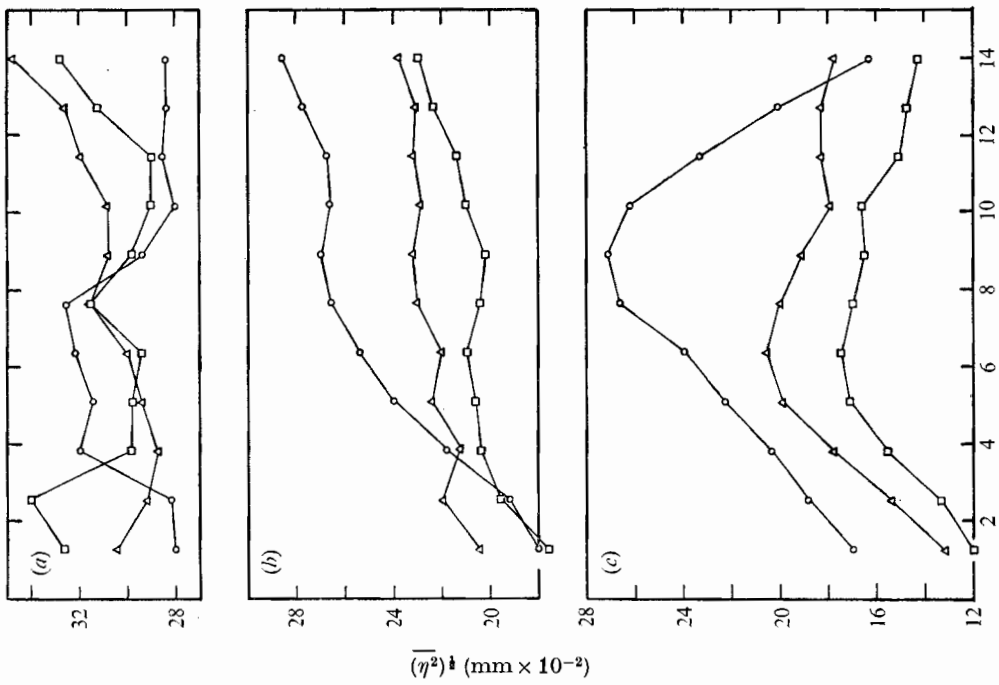

FIGURE 7. Root-mean-square amplitude $(\overline{\eta^2})^{\frac{1}{2}}$ for 4·04 Hz waves expressed as a function of U_r, y and x. (*a*) U_r = 1·84 m/s, run 126. (*b*) U_r = 1·12 m/s, run 132*A*. (*c*) U_r = 0·20 m/s, run 147. Other conditions and symbols as in figure 5.

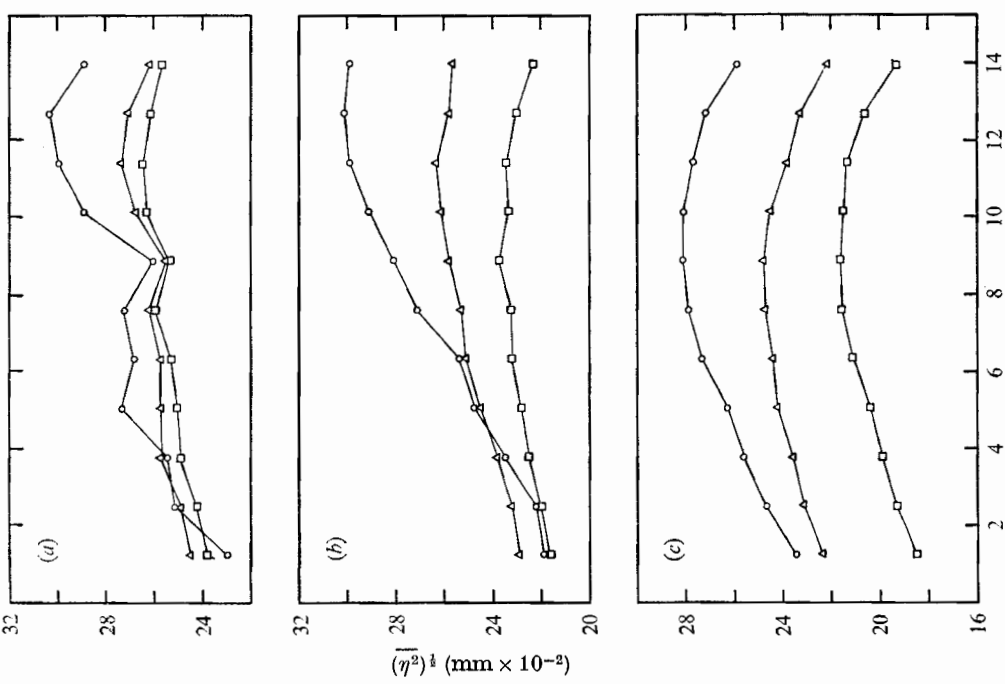

FIGURE 6. Root-mean-square amplitude $(\overline{\eta^2})^{\frac{1}{2}}$ for 3·04 Hz waves expressed as a function of U_r, y and x. (*a*) U_r = 1·84 m/s, run 130. (*b*) U_r = 1·12 m/s, run 131*A*. (*c*) U_r = 0·20 m/s, run 143. Other conditions and symbols as in figure 5.

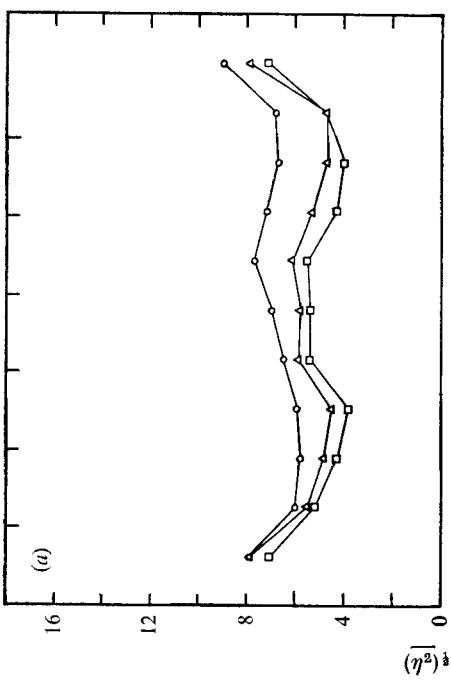

FIGURE 8. Root-mean-square amplitude $(\overline{\eta^2})^{\frac{1}{2}}$ for 5·04 Hz waves expressed as a function of U_r, y and x. (*a*) U_r = 1·84 m/s, run 129*A*. (*b*) U_r = 1·12 m/s, run 133*A*. (*c*) U_r = 0·20 m/s, run 149. Other conditions and symbols as in figure 5.

FIGURE 9. Root-mean-square amplitude $(\overline{\eta^2})^{\frac{1}{2}}$ for 6·04 Hz waves expressed as a function of U_r, y and x. (*a*) U_r = 1·84 m/s, run 129*B*. (*b*) U_r = 1·12 m/s, run 134. (*c*) U_r = 0·20 m/s, run 144. Other conditions and symbols as in figure 5.

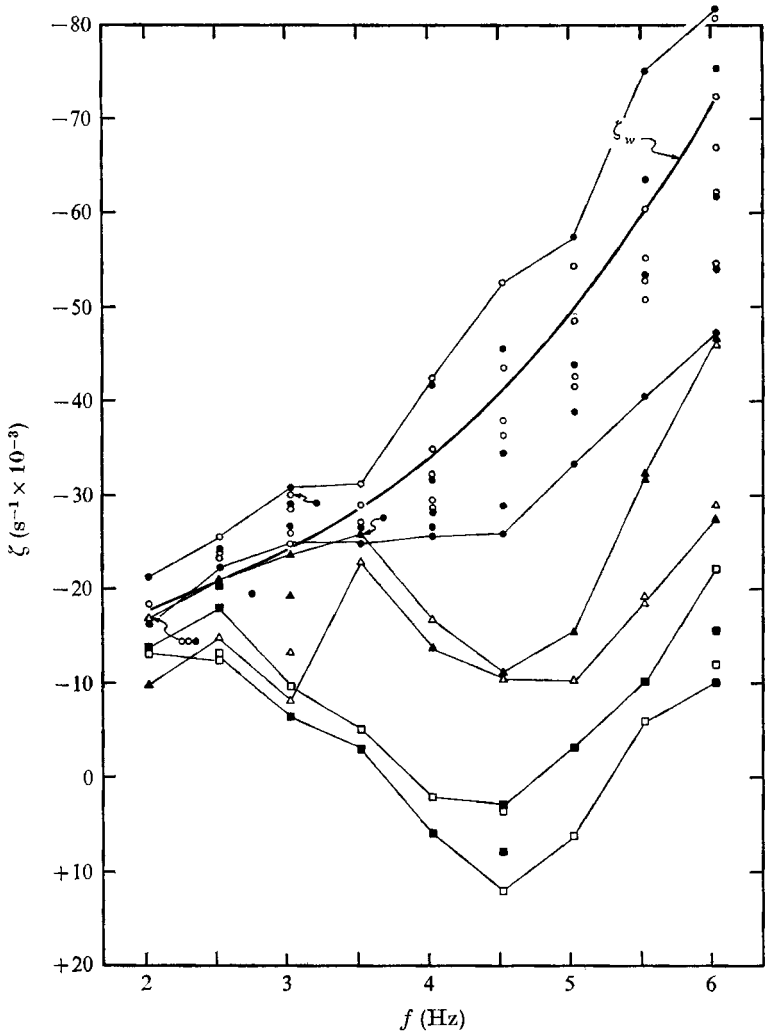

FIGURE 10. Observed (or total) wave growth rates ζ expressed as a function of wave frequency f, centre-line wind velocity U_r and fetch, and theoretical viscous attenuation ζ_w due to bulk and wall effects expressed as a function of wave frequency. Results of all experimental runs have been shown. Open symbols, fetch 1; filled symbols, fetch 2. ○, U_r = 0·20 m/s; △, U_r = 1·12 m/s; □, U_r = 1·84 m/s.

9. Wave growth rates measured experimentally

Observed or total wave growth rates ζ were computed using (5) with the appropriate classical group speed and, as the characteristic amplitude at a particular fetch, the average of the eleven amplitudes across the wave-guide channel. All of these observed wave growth rates are plotted in figure 10. The heavy line represents the theoretical viscous attenuation due to bulk and side-wall effects and was computed using (6), where b = 15·24 cm, the width of the wave-guide channel. When results of duplicate experimental runs were averaged together, it was not possible to distinguish any fetch dependence. The best estimates for

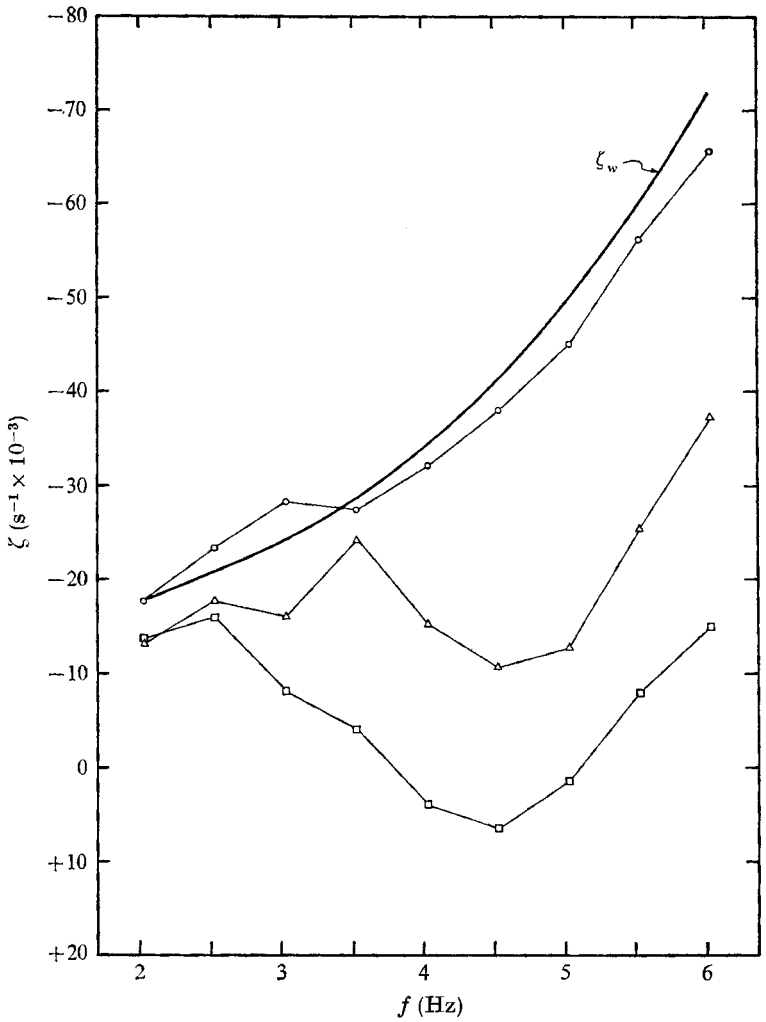

FIGURE 11. Observed (or total) wave growth rates ζ expressed as a function of f and U_r, and theoretical viscous attenuation ζ_w due to bulk and wall effects expressed as a function of f. Results for both fetches have been averaged together. ○, $U_r = 0{\cdot}20$ m/s; △, $U_r = 1{\cdot}12$ m/s; □, $U_r = 1{\cdot}84$ m/s.

the observed wave growth rates, obtained by averaging the results from both fetches, are plotted in figure 11.

In order to have any degree of confidence in the experimental wave measurements, especially in view of the strange amplitude distributions shown in figures 6–8, it was thought *essential* that (i) experimentally measured and theoretically predicted attenuation rates be consistent, and (ii) experimentally measured attenuation rates be independent of wind speed at the lowest frequencies for which the wind-induced growth rates are negligible. Previous investigators [Davies & Vose (1965) considered viscous dissipation due only to bulk effects over a frequency range from 50 to 920 Hz and Van Dorn (1966) considered bulk, side-wall and bottom effects for 0·5 to 2·2 Hz] had demonstrated close agreement

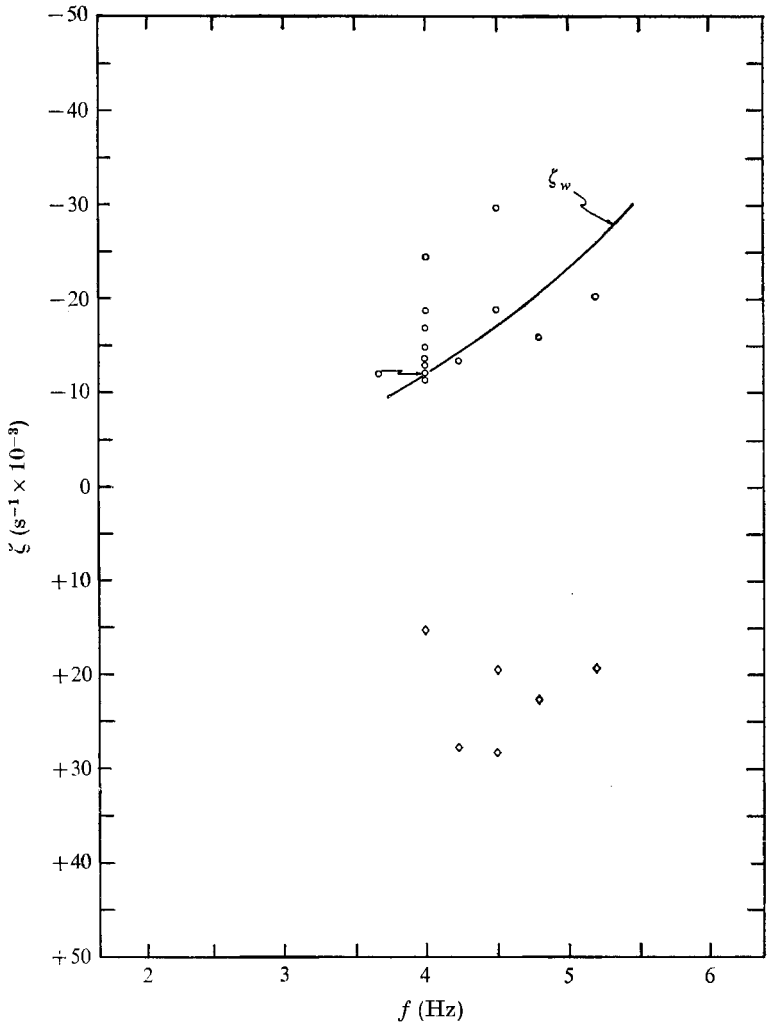

FIGURE 12. Observed (or total) wave growth rates ζ, as reported by Hires (1968), expressed as a function of f and U_r, and theoretical viscous attenuation ζ_w due to bulk and wall effects expressed as a function of f. Results of all of his reported experimental runs have been shown. ○, $U_r = 0$; ◇, $U_r = 1{\cdot}20$.

between experimental and theoretical attenuation rates. All three of these investigators, in addition to McGoldrick (1970), who worked over a frequency range including 9 and 18 Hz, have emphasized the necessity of maintaining a *scrupulously* clean water surface, if close agreement is to be attained. The installation of a stand-pipe drain, the continual addition of water and a wind speed of 0·20 m/s (as mentioned above) were sufficient to ensure a clean water surface and permit measurements which demonstrate the close agreement between experimental and theoretical attenuation rates (see figure 11). For wind speeds slower than 0·20 m/s, the experimental attenuation rates were significantly increased; this is probably due to the fact that surface contaminants were not blown down the tank and skimmed off.

Considering the second essential point, note in figure 11 that towards lower frequencies the three observed wave growth rate curves converge on the theoretical wave attenuation rate curve. This demonstrates, at least for wave frequencies of $2\frac{1}{2}$ Hz and lower, that the wind-induced growth is negligible and that the experimental attenuation rates are independent of wind speed, when

$$0{\cdot}20 \leqslant U_r \leqslant 1{\cdot}84\,\text{m/s}.$$

Miles's theory predicts temporal wave growth rates. To compute temporal growth rates from the spatial measurements made in this study, the wave group velocity c_g must be used (see equation (5)). A certain degree of error has been introduced into the measured growth rates owing to the presence of the wind blowing over the waves. A surface drift current is induced by the wind and the velocity of energy propagation, the wave group velocity, is increased. At the present time no theory exists for estimating this increased or 'effective' group velocity c_{ge}, although both Hidy & Plate (1966) and Gottifredi & Jameson (1970) have made attempts in this direction.

Wu (1968) has made surface drift current measurements and for the range of wind velocities used in this study has suggested that the velocity of the wind-induced drift current *at the surface* of the water is 2–$2\frac{1}{2}$ % of U_r. Assuming that the 'effective' increase in the group velocity is half the surface drift current, then for the following wave frequencies the 'effective' increase $(c_{ge}-c_g)/c_g$ for $U_r = 1{\cdot}84$ m/s would be 6, 11 or 13 % for $f = 2$, 4 or 6 Hz respectively. It would be smaller for $U_r = 1{\cdot}12$ m/s. As will be evident in the final figure, this effect is small compared with the difference between theory and experiment.

10. Wave growth rates from previous experimental work

The only previous experimental work with which the results of this study might reasonably be compared is that of Hires (1968) and Gottifredi & Jameson (1970). For Hires's work, wind-induced growth rates had to be recomputed using the theoretical viscous attenuation due to bulk and side-wall effects; bulk effects only had been considered. Although Hires's experimental apparatus was modified and improved in various ways for use in this study, his results (shown in figure 12) will be included in the comparison of theoretically predicted and experimentally measured growth rates in the next section.

Gottifredi & Jameson (1970) also neglected to include side-wall effects when calculating ζ_w. Their experimental wind-induced growth rates (shown in figure 13) are two to three times *larger* than those obtained in this study. For the reasons cited earlier no further consideration will be given to their work.

11. Comparison of theoretical and experimental growth rates

The wind-induced wave growth rates measured experimentally in this study (computed using the theoretical attenuation rates) and the corresponding growth rates predicted theoretically by Miles's theory have both been plotted in figure 14. For the range of wave frequencies (2·04–6·04 Hz) and the two centre-line wind

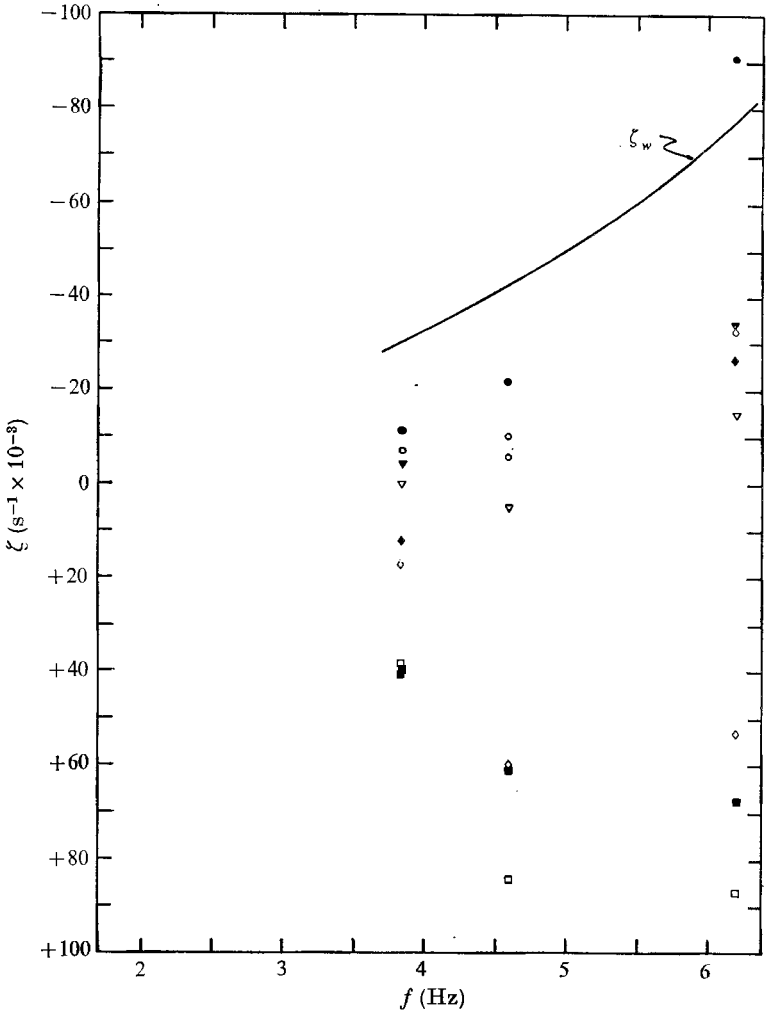

FIGURE 13. Observed (or total) wave growth rates ζ, as reported by Gottifredi & Jameson (1970), expressed as a function of f, U_r and fetch, and theoretical viscous attenuation ζ_w due to bulk and wall effects expressed as a function of f. Only their results for 7·62 Hz have been omitted. Open symbols, fetch 1; filled symbols, fetch 2. ○, $U_r = 0$; ▽, $U_r \sim 0{\cdot}8$ m/s; ◇, $U_r \sim 1{\cdot}5$ m/s; □, $U_r \sim 1{\cdot}9$ m/s.

velocities (1·12 and 1·84 m/s), Miles's theory predicts growth rates which are at least a factor of two larger than those measured experimentally.

The peak in the theoretically predicted growth rate curves for $U_r = 1{\cdot}12$ m/s is interpreted by Miles as a resonance between the water waves and the Tollmien–Schlichting waves in the sheared airflow blowing over the waves. In the experimentally measured curves there is no evidence for such resonance.

The discrepancy between experimental measurements and theoretical predictions can be possibly attributed to certain fundamental assumptions associated with Miles's theory. The theory assumes that the extraction of energy owing to wave growth does not affect the airflow. For this study, this is a good

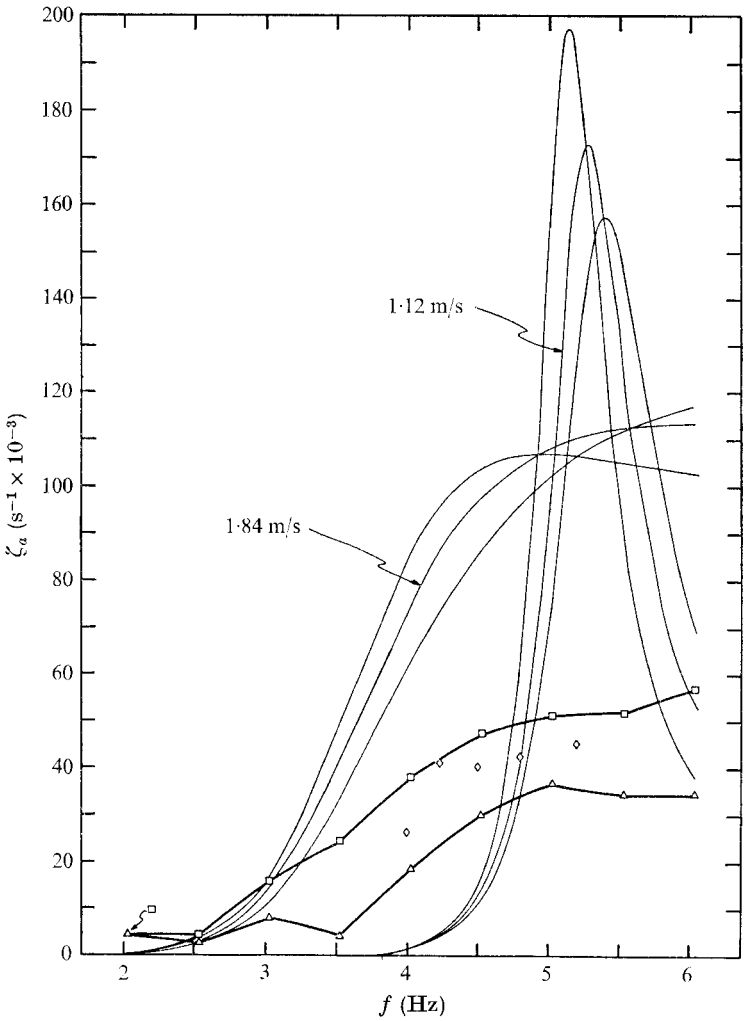

FIGURE 14. A comparison between the wind-induced (or net) wave growth rates ζ_a expressed as a function of f and U_r. Smooth curves represent values predicted by Miles's (1962*b*) theory for this study. Experimentally measured values: △, U_r = 1·12 m/s, this study; □, U_r = 1·84 m/s, this study; ◇, U_r = 1·20 m/s, Hires (1968).

assumption as the ratio of wave-supported shear stress to total shear stress varied only from 0·03 to 3 %. The theory assumes that there is no wind-induced surface drift current. Davis (1972) notes that the momentum flux to the waves depends on the boundary conditions imposed on the airflow by the waves. In addition to altering the group velocity of the waves, the surface drift current alters the airflow close to the water surface, changing the boundary conditions there. Although the surface drift assumption may not be particularly good, the most critical one assumes that the turbulent stresses are not modified by the wavy water surface. Davis (1970, 1972) has shown that the central question concerning the flux of energy from the airflow to the waves involves the wave-induced modifications to the turbulent stresses.

Stanley Corrsin, Blair Kinsman, Larry McGoldrick and Owen Phillips provided much guidance, assistance and encouragement during the course of this study. Support was given by the Office of Naval Research of the Department of the Navy under contract N000 14-67-A-0163-0006, research project NR 083-016.

REFERENCES

BENJAMIN, T. B. 1959 Shearing flow over a wavy wall. *J. Fluid Mech.* **6**, 161–205.

BENJAMIN, T. B. & URSELL, F. 1954 The stability of the plane free surface of a liquid in vertical periodic motion. *Proc. Roy. Soc.* A **225**, 505–515.

COMTE-BELLOT, G. 1965 Écoulement turbulent entre deux parois parallèles. *Publ. Sci. Tech. Min. de l'Air*, no. 419.

DAVIES, J. T. & VOSE, R. W. 1965 On the damping of capillary waves by surface films. *Proc. Roy. Soc.* A **286**, 218–234.

DAVIS, R. E. 1970 On the turbulent flow over a wavy boundary. *J. Fluid Mech.* **42**, 721–732.

DAVIS, R. E. 1972 On prediction of the turbulent flow over a wavy boundary. *J. Fluid Mech.* **52**, 287–306.

DOBSON, F. W. 1971 Measurements of atmospheric pressure on wind-generated sea waves. *J. Fluid Mech.* **48**, 91–127.

GASTER, M. 1971 Vortex shedding from circular cylinders at low Reynolds numbers. *J. Fluid Mech.* **46**, 749–756.

GOTTIFREDI, J. C. & JAMESON, G. J. 1970 The growth of short waves on liquid surfaces under the action of wind. *Proc. Roy. Soc.* A **319**, 373–397.

HIDY, G. M. & PLATE, E. J. 1966 Wind action on water standing in a laboratory channel. *J. Fluid Mech.* **26**, 651–687.

HIRES, R. I. 1968 An experimental study of wind–wave interactions. *Chesapeake Bay Inst., The Johns Hopkins Univ. Tech. Rep.* no. 37.

HUNT, J. N. 1952 Viscous damping of waves over an inclined bed in a channel of finite width. *Houille Blanche*, **7**, 836–842.

HUSSAIN, A. K. M. F. & REYNOLDS, W. C. 1970 The mechanics of a perturbation wave in turbulent shear flow. *Dept. Mech. Engng, Stanford Univ. Rep.* FM-6.

LAUFER, J. 1951 Investigation of turbulent flow in a two-dimensional channel. *N.A.C.A. Rep.* no. 1053.

MCGOLDRICK, L. F. 1965 Wave measurement systems. *Gravitohydrodynamics Lab. Mech. Dept., The Johns Hopkins Univ. Rep.* no. 1.

MCGOLDRICK, L. F. 1970 An experiment on second-order capillary–gravity resonant wave interactions. *J. Fluid Mech.* **40**, 251–271.

MILES, J. W. 1957 On the generation of surface waves by shear flows. *J. Fluid Mech.* **3**, 185–204.

MILES, J. W. 1959*a* On the generation of surface waves by shear flows. Part 2. *J. Fluid Mech.* **6**, 568–582.

MILES, J. W. 1959*b* On the generation of surface waves by shear flows. Part 3. Kelvin–Helmholtz instability. *J. Fluid Mech.* **6**, 583–598.

MILES, J. W. 1962*a* A note on the inviscid Orr–Sommerfeld equation. *J. Fluid Mech.* **13**, 427–432.

MILES, J. W. 1962*b* On the generation of surface waves by shear flows. Part 4. *J. Fluid Mech.* **13**, 433–448.

MILES, J. W. 1967 On the generation of surface waves by shear flows. Part 5. *J. Fluid Mech.* **30**, 163–175.

MONIN, A. S. & YAGLOM, A. M. 1971 *Statistical Fluid Mechanics: Mechanics of Turbulence*, vol. 1. (ed. J. L. Lumley). M.I.T. Press.

OWER, E. & PANKHURST, R. C. 1966 *The Measurement of Air Flow.* Pergamon.

PHILLIPS, O. M. 1957 On the generation of waves by turbulent wind. *J. Fluid Mech.* **2**, 417–445.

PHILLIPS, O. M. 1966 *The Dynamics of the Upper Ocean.* Cambridge University Press.

SUTHERLAND, A. J. 1968 Growth of spectral components in a wind-generated wave train. *J. Fluid Mech.* **33**, 545–560.

URSELL, F. 1952 Edge waves on a sloping beach. *Proc. Roy. Soc.* A **214**, 79–97.

URSELL, F. 1956 Wave generation by wind. In *Surveys in Mechanics* (ed. G. K. Batchelor), pp. 216–249. Cambridge University Press.

VAN DORN, W. G. 1966 Boundary dissipation of oscillatory waves. *J. Fluid Mech.* **24**, 769–779.

WILSON, W. S. 1972 An experimental study of the growth of mechanically generated surface water waves when subjected to a fully developed turbulent channel airflow. *Chesapeake Bay Inst., The Johns Hopkins Univ. Tech Rep.* no. 74.

WU, J. 1968 Laboratory studies of wind–wave interactions. *J. Fluid Mech.* **34**, 91–111.